Research on the Influence Model of Collimating Lens Aberrations in Autocollimation System Based on the Ray-Tracing Method

Jian Shi, Yuechao Li, Daixi Zhang, Heyang Xing, Zixi Tao, and Jiubin Tan

***Abstract*—An influence model of collimating lens aberrations in an autocollimation system based on the ray-tracing method is established. With the ray-tracing method, this model can accurately compute the direction and position of each light ray passing through the collimating lens in an autocollimation system, thereby obtaining the light-spot position of each light ray on the sensor and determining the systematic error caused by aberrations. Eventually, this model serves to compensate for the measurement error of autocollimators and improve the accuracy. Simulations and experiments demonstrate that the influence quantity of angular measurement value due to aberrations reaches 0.74 arcsec within the range of ±500 arcsec. Also, in a large-aberration situation, the measurement accuracy is promoted to 3.33 arcsec, approximately five times higher than that without compensation.**

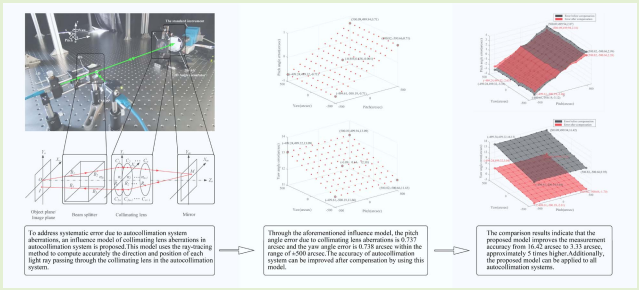

***Index Terms*— Angular measurement accuracy, autocollimation system, collimating lens aberrations, influence model, ray-tracing method.**

I. Introduction

THE autocollimator is an instrument typically used for precision small-angle measurement [1], [2], [3], [4]. It is extensively adopted in precision motion control [5], [6], [7], surface metrology [8], [9], [10], scientific research [11], [12], [13], [14], [15], [16], [17], and other fields. However, in recent years, with an increasing demand for high-precision angle measurement from the engineering community [18], [19], [20], [21], the issue of autocollimator systematic errors caused by measurement models has gradually emerged. Therefore, the key for better angular measurement accuracy lies in the creation of an improved measurement model of autocollimation systems.

Globally, extensive research has been conducted to improve the measurement model of autocollimation systems. Konyakhin et al. [22], [23] developed a ray-tracing autocollimation model for the influence of vignetting. This model can predict the illuminance distribution and calculate the vignetting error. The error caused by vignetting was 3 arcsec with a working distance of 5 m and a range of 60 arcsec. Huang et al. [24] implemented a theoretical autocollimation model based on vector operation to analyze the coupling relationship between 2-D angles. Experiments revealed that the accuracy was improved from 1.71 to 1.55 arcsec after compensation. Zhu et al. [25], [26] established a model of autocollimation system based on matrix optics. It is used to derive the relations between the angular measurement values and the angular drift of the light source, which helps to realize the synchronous compensation technique and achieve the stability of 0.085 arcsec. Shimizu et al. [27] proposed a theoretical autocollimation model based on wave optics. This model indicated that when affected by spherical aberrations in an optical system, the sensor sensitivity of autocollimation system is considerably degraded. In summary, building a more accurate measurement model can enhance the accuracy without increasing the device complexity. However, the existing theoretical autocollimation models based on geometric optics, assuming the collimating

Manuscript received 17 October 2022; revised 20 November 2022; accepted 20 November 2022. Date of publication 2 December 2022; date of current version 12 January 2023. This work was supported in part by the National Key R&D Program of China under Grant 2022YFF0606000 and in part by the National Natural Science Foundation of China under Grant 51405107 and Grant 51775149. The associate editor coordinating the review of this article and approving it for publication was Prof. Santosh Kumar. *(Corresponding author: Jiubin Tan.)*

The authors are with the Center of Ultra-Precision Optoelectronic Instrument Engineering and the Key Laboratory of Ultra-Precision Intelligent Instrumentation, Ministry of Industry and Information Technology, Harbin Institute of Technology, Harbin 150080, China (e-mail: 17B901025@stu.hit.edu.cn; 21S001043@stu.hit.edu.cn; 1190300804@stu.hit.edu.cn; 1190300702@stu.hit.edu.cn; 1190301001@stu.hit.edu.cn; jbtan@hit.edu.cn).

Digital Object Identifier 10.1109/JSEN.2022.3224730

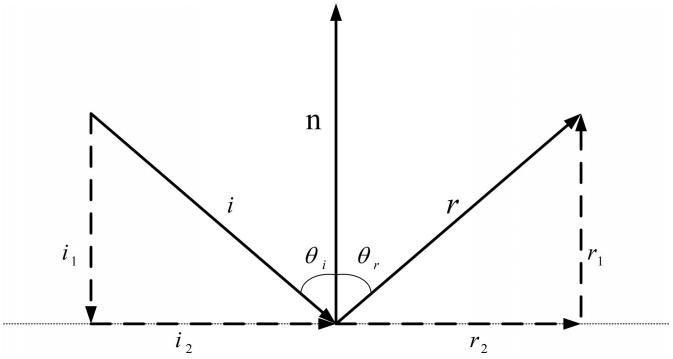

Fig. 1. Schematic of the law of reflection.

lens as an ideal thin lens, have ignored the influence of collimating lens aberrations. Furthermore, the existing models based on wave optics have merely addressed the influence of spherical aberrations on sensor sensitivity, yet its relation with measurement accuracy remains unclear. Therefore, these above models cannot analyze the influence of all kinds of aberrations. Also, the systematic error of autocollimation systems caused by collimating lens aberrations is hard to be solved fundamentally.

In this study, an influence model of collimating lens aberrations in an autocollimation system based on the ray-tracing method is first proposed to solve the aforementioned issues through instrument digitization. Based on the vector expressions of the laws of refraction and reflection, this model applies the ray-tracing method to accurately compute the direction and position of each light ray passing through the collimating lens in the autocollimation system, with the view of deriving the systematic error due to collimating lens aberrations and eventually improving the measurement accuracy by compensation. This model can analyze the influence of all kinds of aberrations and provide a basis for the optimization direction of collimating lens. In addition, it can be applied to all autocollimation systems, which introduces a fresh idea to improve the accuracy of autocollimation techniques.

II. Principle

A. Vector Form of Propagation Theory in Geometric Optics

To establish the influence model, it is necessary to calculate the direction and position of each light ray in autocollimation systems accurately. Moreover, the computational efficiency of the simulation model can be improved by utilizing the propagation theory of the vector form and matrix programming ideas. Hence, this section uses the scalar form of propagation theory in geometric optics to derive the vector form of propagation theory, thereby providing the basis for building the ray-tracing model.

1) Law of Reflection: The law of reflection states that the incident light and the reflected light in the same medium are symmetrically distributed on both sides of the normal line, as shown in Fig. 1, and the scalar expression is

$$\theta_i = \theta_r \tag{1}$$

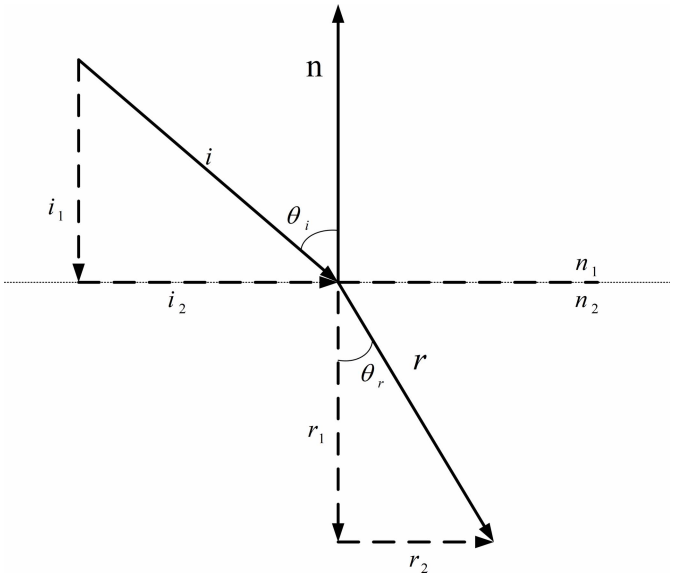

Fig. 2. Schematic of the law of refraction.

where θ_i and θ_r represent the angle between the incident light and the normal line, as well as the angle between the reflected light and the normal line, respectively.

If the unit vector of the incident light is $\vec{i}$, the unit vector of the reflected light is $\vec{r}$, the components in the vertical direction are $\vec{i_1}$ and $\vec{r_1}$, and the components in the horizontal direction are $\vec{i_2}$ and $\vec{r_2}$. According to (1), their relations can be written as follows:

$$\begin{cases} \vec{i} = \vec{i}_1 + \vec{i}_2 \\ \vec{r} = \vec{r}_1 + \vec{r}_2 \\ \vec{r}_1 = -\vec{i}_1 \\ \vec{r}_2 = \vec{i}_2. \end{cases} \tag{2}$$

If the unit normal vector of the medium surface at the incident point is $\vec{n}$, the component $\vec{i_1}$ of the incident light in the normal direction is

$$\vec{i}_1 = -|\vec{i}_1|\vec{n} = \left(\vec{i} \cdot \vec{n}\right)\vec{n}. \tag{3}$$

The vector form of the law of reflection can be derived from (2) and (3), and the equation of the unit vector $\vec{r}$ of the reflected light is

$$\vec{r} = \vec{i} - 2(\vec{i} \cdot \vec{n})\vec{n}. \tag{4}$$

2) Law of Refraction: The schematic of the law of refraction is presented in Fig. 2 and its scalar form is

$$n_1 \sin\theta_i = n_2 \sin\theta_r \tag{5}$$

where θ_i and θ_r denote the angle between the incident light and the normal line, and the angle between the refracted light and the normal line, respectively, and n_1 and n_2 denote the refractive index of the two media before and after light refraction, respectively.

If the unit vector of the incident light is $\vec{i}$, the unit vector of the refracted light is $\vec{r}$, the components in the vertical

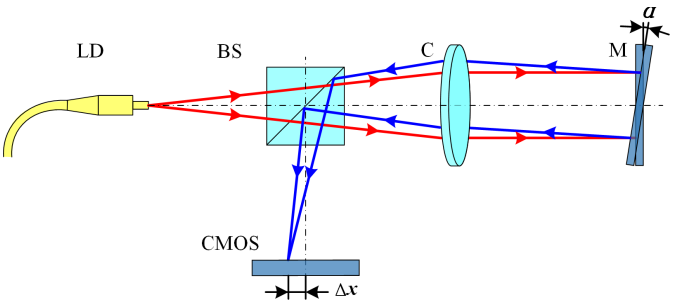

Fig. 3. Schematic of autocollimation system.

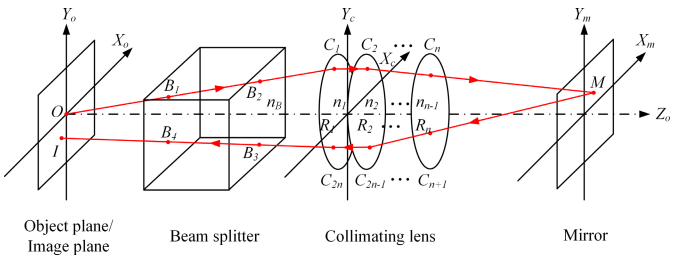

Fig. 4. Schematic of the influence model based on the ray-tracing method.

direction are $\overrightarrow{i_1}$ and $\overrightarrow{r_1}$, the components in the horizontal direction are $\overrightarrow{i_2}$ and $\overrightarrow{r_2}$, and the unit normal vector of the medium surface at the incident point is $\overrightarrow{n}$. They have the following relations:

$$\begin{cases} \vec{i} = \vec{i}_1 + \vec{i}_2 \\ \vec{r} = \vec{r}_1 + \vec{r}_2 \\ |\vec{i}|^2 = |\vec{i}_1|^2 + |\vec{i}_2|^2 = 1 \\ |\vec{r}|^2 = |\vec{r}_1|^2 + |\vec{r}_2|^2 = 1. \end{cases} \tag{6}$$

According to (5) and (6), the components $\overrightarrow{r_1}$ and $\overrightarrow{r_2}$ of the unit vector $\overrightarrow{r}$ of the refracted light can be calculated by the following equations:

$$\vec{r}_1 = -\vec{n}\sqrt{1 - \left(\frac{n_1}{n_2}\right)^2 \left(1 - \left(\vec{i} \cdot \vec{n}\right)^2\right)} \tag{7}$$

$$\vec{r}_2 = \frac{n_1}{n_2}(\vec{i} - (\vec{i} \cdot \vec{n})\vec{n}). \tag{8}$$

Eventually, the vector form of the law of refraction can be derived from (7) and (8), and the equation of the unit vector $\overrightarrow{r}$ of the refracted light is given by

$$\vec{r} = \vec{r}_2 + \vec{r}_1 = \frac{n_1}{n_2}\vec{i} - \frac{n_1}{n_2}\left(\vec{i} \cdot \vec{n}\right) + \sqrt{1 - \left(\frac{n_1}{n_2}\right)^2 \left(1 - \left(\vec{i} \cdot \vec{n}\right)^2\right)}\vec{n}. \tag{9}$$

B. Influence Model of Collimating Lens Aberrations in Autocollimation System Based on the Ray-Tracing Method

The schematic of the autocollimation system is presented in Fig. 3. The light from a fiber-coupled laser diode (LD) passes through a beam splitter (BS) and a collimating lens (C). Subsequently, the light collimated by C is projected vertically onto a plane mirror (M). When M is stationary, the reflected light returns along the original path and focuses at the center of the image sensor (CMOS). When M is rotated by an angle α, the direction of the reflected light correspondingly changes. After being reflected by the BS, the light focuses at a position with a displacement of Δx from the center of CMOS. The angular deflection of M can be calculated using the light-spot displacement.

Therefore, according to the schematic presented in Fig. 3 of the autocollimation system, an influence model of collimating lens aberrations in the autocollimation system based on the ray-tracing method is proposed, as shown in Fig. 4.

As the image plane of the sensor and the object plane of the light source are conjugated with each other in space, the image plane in the ray-tracing process is set on the object plane to simplify the model. The coordinate system of the object plane is $X_oO_oY_o$, the coordinate system of the C-plane is $X_cO_cY_c$, the coordinate system of the M-plane is $X_mO_mY_m$, and the position of the object plane $X_oO_oY_o$ is the zero position in the z-direction. A light ray OB_1 from point O is considered as an example. It is first refracted twice by the BS. The intersection points of the light and the front and back surfaces of BS are B_1 and B_2, respectively. Then, it is refracted multiple times by C and intersects with different medium surfaces of the lens group at $C_1, C_2, \ldots, C_n$. Subsequently, the light is reflected by M and intersects with it at point M. Then, the light returns and passes through the collimating lens group and BS (and intersects with the collimating lens group and BS at C_{n+1}, $C_{n+2}, \ldots, C_{2n}$, B_3, and B_4) and finally intersects with the image plane at point I.

If the spatial coordinate of the light source is $O = (0, 0, 0)$, the unit direction vector of the incident light is $\overrightarrow{OB_1} = (x_{OB_1}, y_{OB_1}, z_{OB_1})$, and the plane equation of the front surface of BS is $z = z_{B_1}$, the intersection point B_1 can be calculated by the following equation:

$$\begin{cases} \dfrac{x}{x_{OB_1}} = \dfrac{y}{y_{OB_1}} = \dfrac{z}{z_{OB_1}} \\ z = z_{B_1}. \end{cases} \tag{10}$$

Let $B_1 = (x_{B_1}, y_{B_1}, z_{B_1})$, and the unit normal vector of the front surface of the BS is $\overrightarrow{N_{B_1}} = (0, 0, -1)$. The unit direction vector $\overrightarrow{B_1B_2}$ of the refracted light can be computed by using $\overrightarrow{OB_1}$, $\overrightarrow{N_{B_1}}$, and (9)

$$\overrightarrow{B_1B_2} = \frac{1}{n_B}\overrightarrow{OB_1} - \left(\frac{1}{n_B}\left(\overrightarrow{OB_1} \cdot \overrightarrow{N_{B_1}}\right) + \sqrt{1 - \frac{1}{n_B^2}\left(1 - \left(\overrightarrow{OB_1} \cdot \overrightarrow{N_{B_1}}\right)^2\right)}\right)\overrightarrow{N_{B_1}} \tag{11}$$

where n_B is the refractive index of the BS.

Similarly, the spatial coordinate of B_2 and the unit direction vector of the refracted light B_2C_1 can be determined

$$B_2 = \left(x_{B_2}, y_{B_2}, z_{B_2}\right) \tag{12}$$

$$\overrightarrow{B_2C_1} = n_B\overrightarrow{B_1B_2} - (n_B(\overrightarrow{B_1B_2} \cdot \overrightarrow{N_{B_2}}) + \sqrt{1 - n_B^2(1 - (\overrightarrow{B_1B_2} \cdot \overrightarrow{N_{B_2}})^2)}\overrightarrow{N_{B_2}} \tag{13}$$

where $\overrightarrow{N_{B_2}} = (0, 0, -1)$ is the unit normal vector of the back surface of the BS.

If $\overrightarrow{B_2C_1} = (x_{B_2C_1}, y_{B_2C_1}, z_{B_2C_1})$, the coordinate of the center of the first medium sphere of C is $(0, 0, o_{C_1})$, the radius of this sphere is R_1, and the refractive index is n_1, the coordinate of C_1 can be obtained by (14) and written as (15)

$$\begin{cases} \dfrac{x - x_{B_2}}{x_{B_2C_1}} = \dfrac{y - y_{B_2}}{y_{B_2C_1}} = \dfrac{z - z_{B_2}}{z_{B_2C_1}} \\ x^2 + y^2 + \left(z - o_{C_1}\right)^2 = R_1^2 \end{cases} \tag{14}$$

$$C_1 = (x_{C_1}, y_{C_1}, z_{C_1}). \tag{15}$$

Then, the unit normal vector at C_1 is

$$\overrightarrow{N_{C_1}} = \frac{\overrightarrow{O_{C_1}C_1}}{\left|\overrightarrow{O_{C_1}C_1}\right|} = \frac{\left(x_{C_1}, y_{C_1}, z_{C_1} - o_{C_1}\right)}{\left|\left(x_{C_1}, y_{C_1}, z_{C_1} - o_{C_1}\right)\right|}. \tag{16}$$

Based on (9), the unit direction vector of the light passing through the first medium surface of C can be given as (17), shown at the bottom of the page.

Similarly, the unit direction vector of the light passing through each medium surface of C can be calculated, such as $\overrightarrow{C_2C_3}$ and $\overrightarrow{C_nM}$, (18) and (19) as shown at the bottom of the page, where n_2 and n_{n-1} denote the refractive indices of the medium between the second and third surfaces of C and between the $(n-1)$th and nth surfaces, respectively, and $\overrightarrow{N_{C_2}}$ and $\overrightarrow{N_{C_n}}$ are the unit normal vectors at the point C_2 on the second surface and the point C_n on the nth surface of C, respectively.

When M is perpendicular to the optical axis Z_o of the autocollimation system, the unit normal vector of M is $\overrightarrow{N_{M_0}} = (0, 0, -1)$. When the pitch and yaw angle rotations of M relative to $X_m O_m Y_m$ are α and β, respectively, the unit normal vector $\overrightarrow{N_M}$ of M can be expressed by the Euler rotation as

$$R_x = \begin{bmatrix} 1 & 0 & 0 \\ 0 & \cos\alpha & -\sin\alpha \\ 0 & \sin\alpha & \cos\alpha \end{bmatrix} \tag{20}$$

$$R_y = \begin{bmatrix} \cos\beta & 0 & \sin\beta \\ 0 & 1 & 0 \\ -\sin\beta & 0 & \cos\beta \end{bmatrix} \tag{21}$$

$$\overrightarrow{N_M} = \overrightarrow{N_{M_0}} \cdot R_x \cdot R_y. \tag{22}$$

If $C_n = (x_{C_n}, y_{C_n}, z_{C_n})$, $\overrightarrow{C_nM} = (x_{C_nM}, y_{C_nM}, z_{C_nM})$, and $\overrightarrow{N_M} = (x_{N_M}, y_{N_M}, z_{N_M})$, the spatial coordinate of the intersection point M can be obtained by (23) and expressed by (24)

$$\begin{cases} \dfrac{x - x_{C_n}}{x_{C_nM}} = \dfrac{y - y_{C_n}}{y_{C_nM}} = \dfrac{z - z_{C_n}}{z_{C_nM}} \\ x_{N_M} x + y_{N_M} y + z_{N_M}\left(z - z_{O_M}\right) = 1 \end{cases} \tag{23}$$

$$M = (x_M, y_M, z_M) \tag{24}$$

where z_{O_M} is the Z_o-coordinate of the intersection point of the M plane and the optical axis Z_o.

According to (4), the unit direction vector of the reflected light after being reflected by M can be addressed as

$$\overrightarrow{MC_{n+1}} = \overrightarrow{C_nM} - 2\left(\overrightarrow{C_nM} \cdot \overrightarrow{N_M}\right)\overrightarrow{N_M}. \tag{25}$$

The reflected light returns along the original path and is refracted by C and BS again. Similarly, according to the above equations, the spatial coordinate of the final intersection point I of the light and the image plane can be given as

$$I = (x_I, y_I, z_I). \tag{26}$$

At this time, the ray-tracing process of light ray OB_1 in the autocollimation system is completed. When the simulation generates n light rays, the image point set I can be determined after ray tracing

$$I = \{(x_{Ik}, y_{Ik}, z_{Ik}) \,|k = 1, 2, \ldots, n.; z_{Ik} = 0\}. \tag{27}$$

We have assumed that the light intensity of each light ray in the model is consistent. When the pitch and yaw angle rotations of M are α and β, by using the image point set I and the centroid positioning algorithm, the light-spot displacement on the sensor can be derived as

$$\begin{aligned} \Delta x &= \frac{\sum_{k=1}^{n} x_{Ik} I_{Ik}}{\sum_{k=1}^{n} I_{Ik}} = \frac{\sum_{k=1}^{n} x_{Ik}}{n} \\ \Delta y &= \frac{\sum_{k=1}^{n} y_{Ik} I_{Ik}}{\sum_{k=1}^{n} I_{Ik}} = \frac{\sum_{k=1}^{n} y_{Ik}}{n}. \end{aligned} \tag{28}$$

Based on the measurement principle of the autocollimation system, the measurement values of the pitch and yaw angles can be computed as

$$\begin{aligned} \alpha_{\text{measure}} &= \frac{1}{2}\arctan\left(\frac{\Delta x}{f}\right) \\ \beta_{\text{measure}} &= \frac{1}{2}\arctan\left(\frac{\Delta y}{f}\right). \end{aligned} \tag{29}$$

Subsequently, the angular errors caused by collimating lens aberrations of the autocollimation system can be expressed

$$\overrightarrow{C_1C_2} = \frac{1}{n_1}\overrightarrow{B_2C_1} - \left(\frac{1}{n_1}\left(\overrightarrow{B_2C_1} \cdot \overrightarrow{N_{C_1}}\right) + \sqrt{1 - \frac{1}{n_1^2}\left(1 - \left(\overrightarrow{B_2C_1} \cdot \overrightarrow{N_{C_1}}\right)^2\right)}\right)\overrightarrow{N_{C_1}} \tag{17}$$

$$\overrightarrow{C_2C_3} = \frac{n_1}{n_2}\overrightarrow{C_1C_2} - \left(\frac{n_1}{n_2}\left(\overrightarrow{C_1C_2} \cdot \overrightarrow{N_{C_2}}\right) + \sqrt{1 - \frac{n_1^2}{n_2^2}\left(1 - \left(\overrightarrow{C_1C_2} \cdot \overrightarrow{N_{C_2}}\right)^2\right)}\right)\overrightarrow{N_{C_2}} \tag{18}$$

$$\overrightarrow{C_nM} = n_{n-1}\overrightarrow{C_{n-1}C_n} - \left(n_{n-1}\left(\overrightarrow{C_{n-1}C_n} \cdot \overrightarrow{N_{C_n}}\right) + \sqrt{1 - n_{n-1}^2\left(1 - \left(\overrightarrow{C_{n-1}C_n} \cdot \overrightarrow{N_{C_n}}\right)^2\right)}\right)\overrightarrow{N_{C_n}} \tag{19}$$

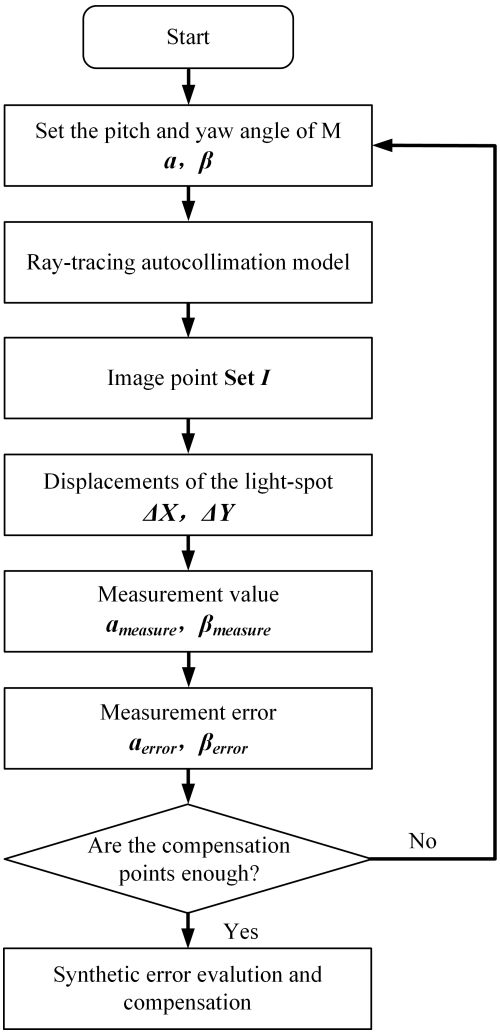

Fig. 5. Flowchart of the influence model based on the ray-tracing method.

as follows:

$$\begin{aligned} \alpha_{\text{error}} &= \alpha_{\text{measure}} - \alpha \\ \beta_{\text{error}} &= \beta_{\text{measure}} - \beta. \end{aligned} \tag{30}$$

In summary, the calculation flowchart of this model is presented in Fig. 5.

The error data can be used to fit the relationship between the angular measurement errors and the theoretical value of angle measurement

$$\begin{cases} \alpha_{\text{error}} &= F(\alpha, \beta) \\ \beta_{\text{error}} &= G(\alpha, \beta). \end{cases} \tag{31}$$

According to (30) and (31), α and β can also be addressed as

$$\begin{cases} \alpha &= \alpha_{\text{measure}} - F(\alpha, \beta) \\ \beta &= \beta_{\text{measure}} - G(\alpha, \beta). \end{cases} \tag{32}$$

Therefore, α and β can be obtained by (32) using α_{measure} and β_{measure}, which is the compensation process of this influence model.

Therefore, through the aforementioned influence model, the angular errors of pitch and yaw angles caused by aberrations can be obtained, which also helps to determine the relationship between aberrations and angular measurement values. Eventually, while guiding the design of collimating lens in an autocollimation system, this model can compensate for the measurement errors and improve the accuracy. The comparisons between previously reported work and the proposed model are presented in Table I. This model does not use thin lens approximation and has the advantage of analyzing the influence of all kinds of aberrations. However, the analytical relationship between aberrations and measurement error cannot be obtained, and the influence can only be calculated through computer simulation of the ray-tracing process.

III. Simulation and Analysis

A. Comparison of the Proposed Model and the Model Based on Zemax

The collimating lens C in the simulation is a doublet lens with a focal length of 500 mm and an aperture of 50.8 mm. Its radii are 289.085, –232.625, and –759.288 mm; the refractive indices of the two materials are 1.5164 (H-K9) and 1.6727 (H-ZF2), and the center thicknesses are 5.5 and 3.5 mm, respectively. The BS is BS013 (Thorlabs, USA) with a size of 25.4 mm and a refractive index of 1.5168 (N-BK7). According to these parameters of optical elements, the simulation model of the autocollimation system based on Zemax is established. The optical system parameters are presented in Table II.

According to the optical system parameters listed in Table II and equations in Section II, an influence model of collimating lens aberrations in an autocollimation system based on the ray-tracing method is written in python on the Pycharm platform. Furthermore, the tracing results of these two models are compared to prove the theoretical correctness of the proposed model. The 2-D layouts of two models are shown in Fig. 6.

If there are nine different pairs of pitch and yaw angle rotations of M, namely,

$$\begin{cases} \alpha = 0'' \\ \beta = 0'', \end{cases} \begin{cases} \alpha = 0'' \\ \beta = 500'', \end{cases} \begin{cases} \alpha = 500'' \\ \beta = 0'', \end{cases}$$

$$\begin{cases} \alpha = 0'' \\ \beta = -500'', \end{cases} \begin{cases} \alpha = -500'' \\ \beta = 0'' \end{cases}, \begin{cases} \alpha = -500'' \\ \beta = -500'', \end{cases}$$

$$\begin{cases} \alpha = 500'' \\ \beta = -500'', \end{cases} \begin{cases} \alpha = -500'' \\ \beta = 500'', \end{cases} \text{and} \begin{cases} \alpha = 500'' \\ \beta = 500'' \end{cases}$$

the spot diagrams of two models are presented in Fig. 7.

The rms radii of the spot diagrams of these two models are shown in Table III.

The comparison among Figs. 6 and 7 and Table III indicates that the tracing results of the proposed model and the model based on Zemax are virtually the same, and the relative error of rms radius is less than 0.87%. This proves the correctness of the proposed influence model.

TABLE I
COMPARISONS BETWEEN PREVIOUSLY REPORTED WORK AND THE PROPOSED MODEL

Time	Name	Method	Research objectives	Is there a thin lens approximation?	Can the model analyze the influence of aberrations?
-	The traditional model	Geometric optics	basic model of autocollimator	Yes	No
2006	Huang et al.	Vector operation	coupling relationship between pitch and yaw	Yes	No
2013	Zhu et al.	Matrix optics	angular drift of the light source	Yes	No
2013	Konyakhin et al.	Ray-tracing	the vignetting	No	Only the vignetting
2016	Gao et al.	Wave optics	the spherical aberration	No	Only the spherical aberration
2022	The model in this paper	Ray-tracing	aberrations	No	All kinds of aberrations

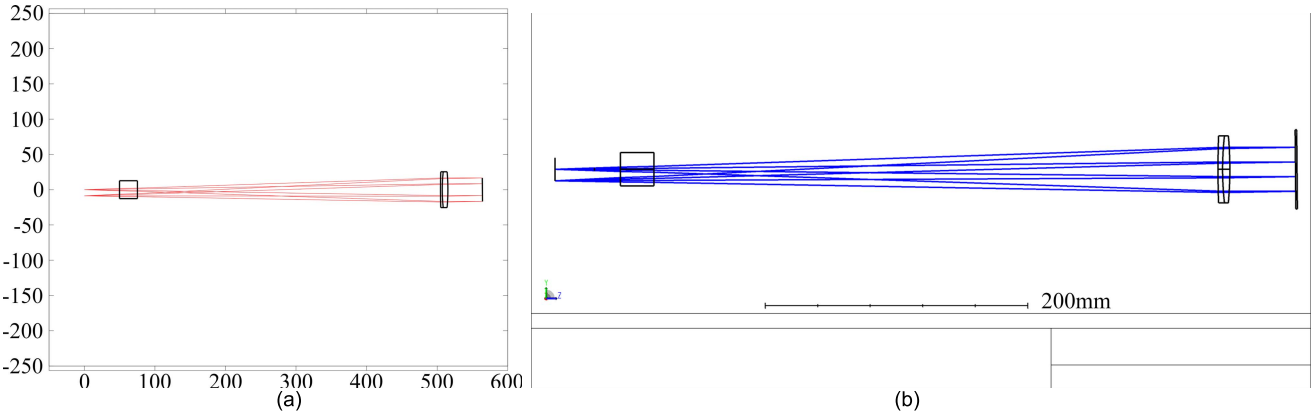

Fig. 6. Two-dimensional layouts of two models (unit: mm). (a) Model proposed in this article. (b) Model based on Zemax.

B. Analysis of the Influence Quantity of Collimating Lens Aberrations

During the simulation, first, the pitch and yaw angle rotations of M are set within a range of ± 500 arcsec and an angular step of 100 arcsec. Second, using the influence model established in Section III-A, the angular measurement values corresponding to the 121 pairs of pitch and yaw angles can be obtained. Finally, the angular measurement errors due to collimating lens aberrations can be calculated, as shown in Fig. 8.

The simulation results have revealed that within the range of ± 500 arcsec, the pitch angle error due to collimating lens aberrations is 0.737 arcsec and the yaw angle error is 0.738 arcsec. Thus, the influence of collimating lens aberrations on the autocollimation system is not negligible. Furthermore, the point with the maximum angular error is located at the edge of the measurement range, and the point with the minimum angular error is located at the origin. This indicates that the influence of lens aberrations on the edge of the range is greater than the influence on the center.

IV. EXPERIMENTS

A. Experimental Setup

To study and verify the proposed influence model, an experimental setup was designed and constructed in a clean room, as shown in Fig. 9. The light source LD was a fiber-coupled LD with a central wavelength of 532 nm and an output power of 10 mW. The CMOS sensor was BFS-U3-32S4M (FLIR, USA), with a resolution of 2048 $\times$ 1536 and a pixel size of 3.45 μm. The collimating lens (C) was the same as that in Section III-A. The reflective target was composed of a 2-D angle generator (2-D-AG) and a plane mirror (M), while the 2-D-AG was New Focus 8824-AC (Newport, USA).

B. Accuracy Test Before and After Using the Influence Model for Compensation

To prove that the proposed model can improve the measurement accuracy and reduce the error arising from collimating lens aberrations, an accuracy test on the autocollimation system before and after using this model for compensation was conducted.

As shown in Fig. 10, a standard instrument and the autocollimation system were simultaneously used to measure the 2-D small-angle deviations of M. Furthermore, this test selected the experimental data of the standard instrument as the true value and compared the measurement errors before and after using the proposed model for compensation. The standard instrument employed in this experiment was a two-dimensional photoelectric autocollimator (Möller-Wedel Elcomat 3000, Germany),

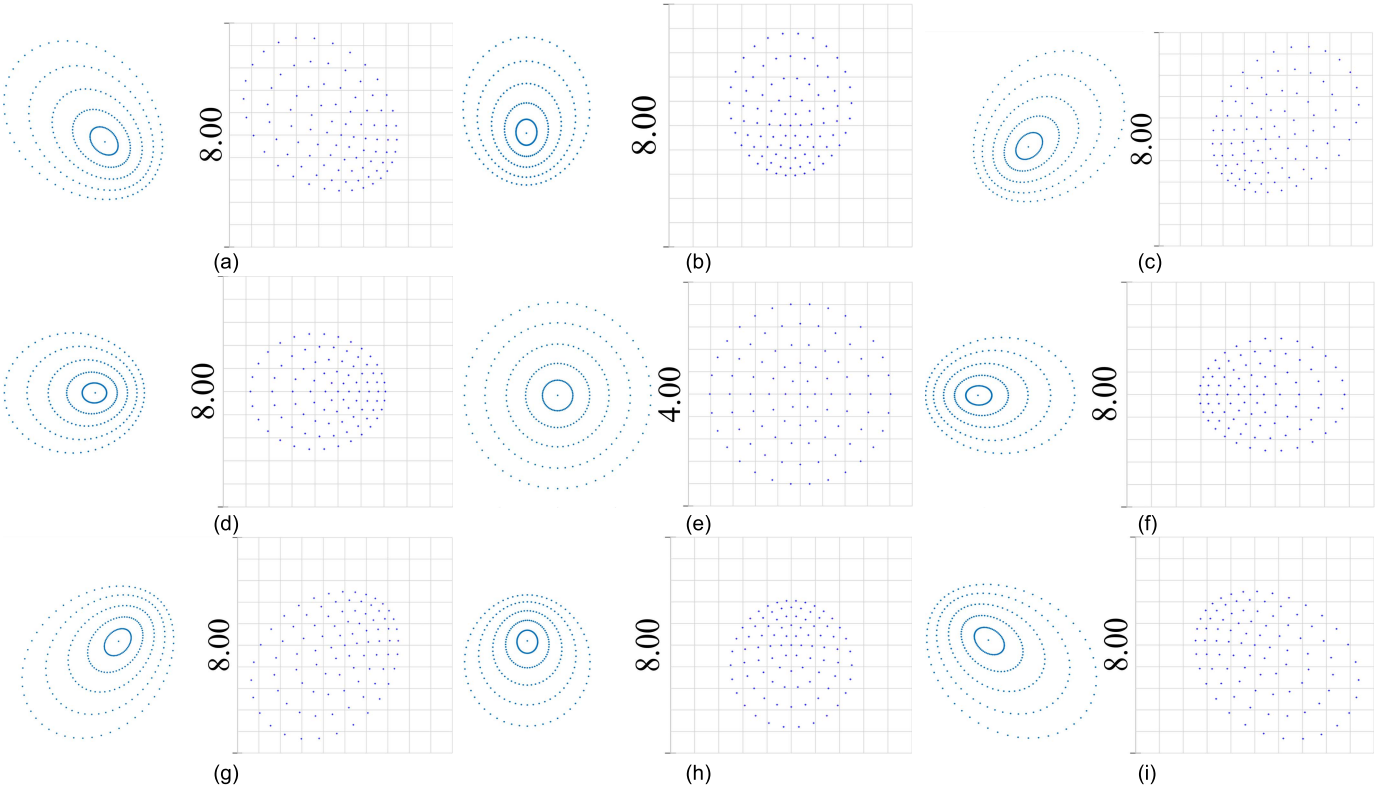

Fig. 7. Spot diagrams of two models (left: proposed model; right: model based on Zemax, unit: μm). (a) $\alpha = -500$ arcsec and $\beta = -500$ arcsec. (b) $\alpha = -500$ arcsec and $\beta = 0$ arcsec. (c) $\alpha = -500$ arcsec and $\beta = 500$ arcsec. (d) $\alpha = 0$ arcsec and $\beta = -500$ arcsec. (e) $\alpha = 0$ arcsec and $\beta = 0$ arcsec. (f) $\alpha = 0$ arcsec and $\beta = 500$ arcsec. (g) $\alpha = 500$ arcsec and $\beta = -500$ arcsec. (h) $\alpha = 500$ arcsec and $\beta = 0$ arcsec. (i) $\alpha = 500$ arcsec and $\beta = 500$ arcsec.

TABLE II
LENS DATA OF THE MODEL BASED ON ZEMAX

Surf:	Type	Comment	Radius (mm)	Thickness (mm)	Glass	Semi-D (mm)
OBJ	Standard	-	Infinity	30.000	-	0.000
1	Standard	D	Infinity	19.882	-	1.000
2	Standard	BS	Infinity	25.400	N-BK7	12.700
3	Standard	-	Infinity	429.762	-	12.700
4	Standard	C	759.288	3.500	H-ZF2	25.400
5	Standard	C	232.655	5.500	H-K9	25.400
6	Standard	-	-289.085	50.000	-	25.400
7	Coordinate break	-	Infinity	0.000	-	0.000
8	Standard	M	Infinity	0.000	Mirror	30.000
9	Coordinate break	-	Infinity	0.000	-	0.000
10	Coordinate break	-	Infinity	-50.000	-	0.000
11	Standard	C	-289.085	-5.500	H-K9	25.400
12	Standard	C	232.655	-3.500	H-ZF2	25.400
13	Standard	-	759.288	-429.762	-	25.400
14	Standard	BS	Infinity	-25.400	N-BK7	12.700
15	Standard	-	Infinity	-49.882	-	12.700
IMA	Standard	-	Infinity	-	-	1.011 E-003

TABLE III
RMS RADIUS OF SPOT DIAGRAM OF TWO MODELS

Serial number	Angles produced by M		RMS Radius(μm)	
	Pitch(arcsec)	Yaw(arcsec)	Zemax	Python
1	0	0	1.120	1.129
2	0	500	1.540	1.553
3	0	-500	1.541	1.553
4	500	0	1.540	1.553
5	-500	0	1.541	1.553
6	500	500	1.955	1.972
7	500	-500	1.956	1.972
8	-500	500	1.957	1.972
9	-500	-500	1.957	1.972

with a resolution of 0.05 arcsec and a measurement accuracy of ± 0.1 arcsec within the range of 20 arcsec.

In the experiment, C was fixed on a precision linear stage (LS), which moved 0.03 mm in the x-direction, to create a large-aberration situation of the autocollimation system. Moreover, the controller made the 2-D-AG drive M to produce angles. Within the range of ± 500 arcsec and a step of 100 arcsec, the autocollimation system and the standard instrument simultaneously collected 121 pairs of pitch and yaw angles. Then, through the proposed influence model, the angular measurement errors for the 121 pairs of pitch and yaw angles can be calculated, as shown in Fig. 11.

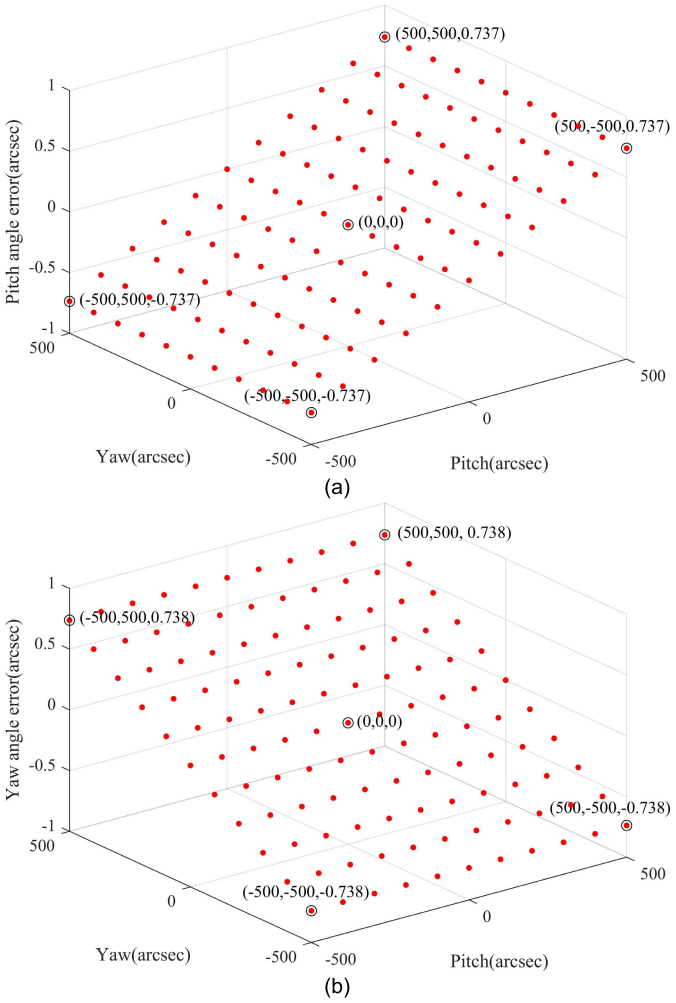

Fig. 8. Angular errors calculated by the influence model. (a) Pitch angle error. (b) Yaw angle error.

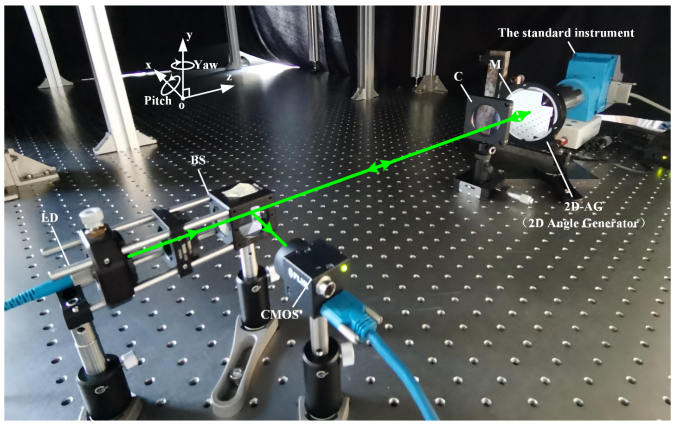

Fig. 9. Photograph of the high-precision autocollimation experimental setup for verifying the proposed model.

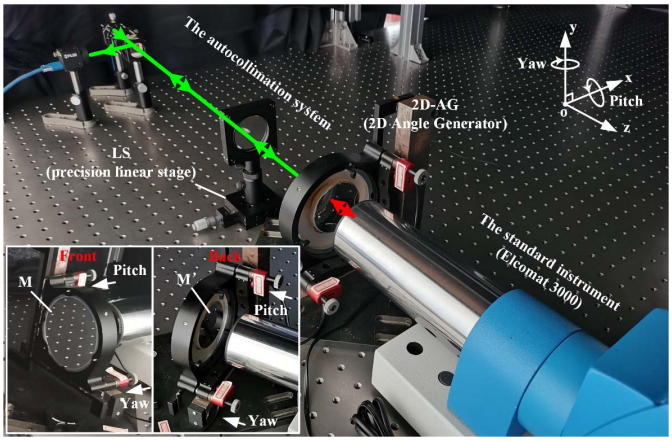

Fig. 10. Setup for the accuracy test.

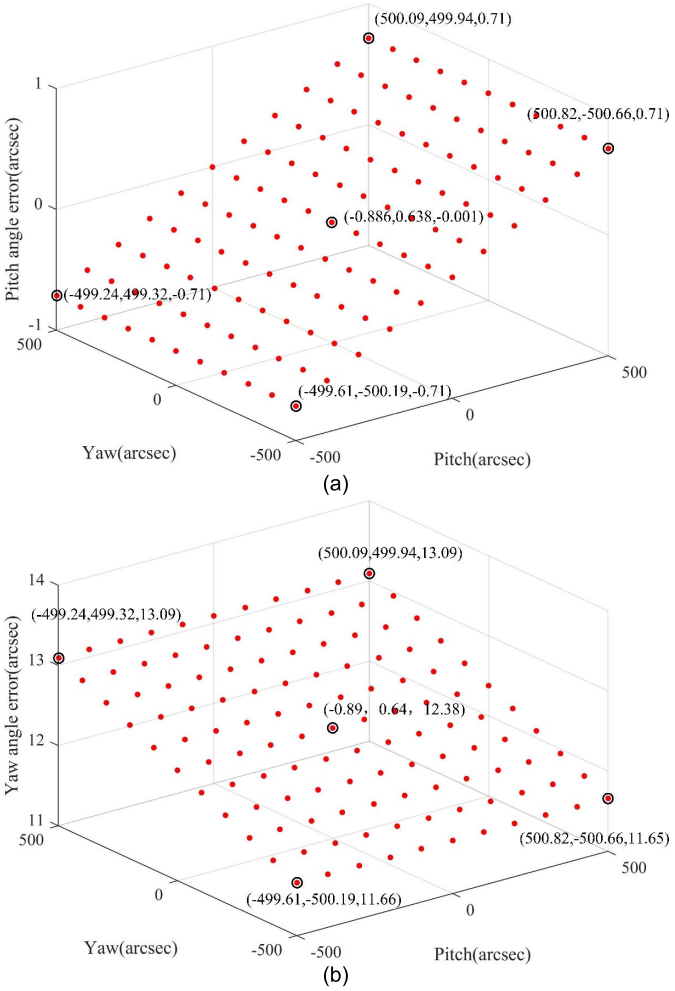

Fig. 11. Angular errors due to collimating lens aberrations in the experiment. (a) Pitch angle error. (b) Yaw angle error.

The accuracy results without using the proposed model for compensation are presented in black in Fig. 12(a) and (b). The maximum deviations of pitch and yaw angles are –3.34 and 16.42 arcsec, respectively. Using this proposed model, the maximum deviations of pitch and yaw angles are –2.63 and 3.33 arcsec, respectively, as shown in red in Fig. 12(a) and (b). The comparison results in Fig. 12 and Table IV indicate that the proposed model promotes the measurement accuracy from 16.42 to 3.33 arcsec, approximately five times higher.

TABLE IV
COMPARISONS BETWEEN TWO TRADITIONAL MODELS AND THE PROPOSED MODEL

Name	Method	Minimum error of pitch (arcsec)	Maximum error of pitch (arcsec)	Minimum error of yaw (arcsec)	Maximum error of yaw (arcsec)
The traditional model I	$\alpha=\frac{\Delta x}{2f}$ $\beta=\frac{\Delta y}{2f}$	2.882	-3.353	9.642	16.429
The traditional model II	$\alpha=\frac{1}{2}\arctan(\frac{\Delta x}{f})$ $\beta=\frac{1}{2}\arctan(\frac{\Delta y}{f})$	2.878	-3.349	9.645	16.425
The model in this paper	Ray-tracing	2.162	-2.635	-1.707	3.331

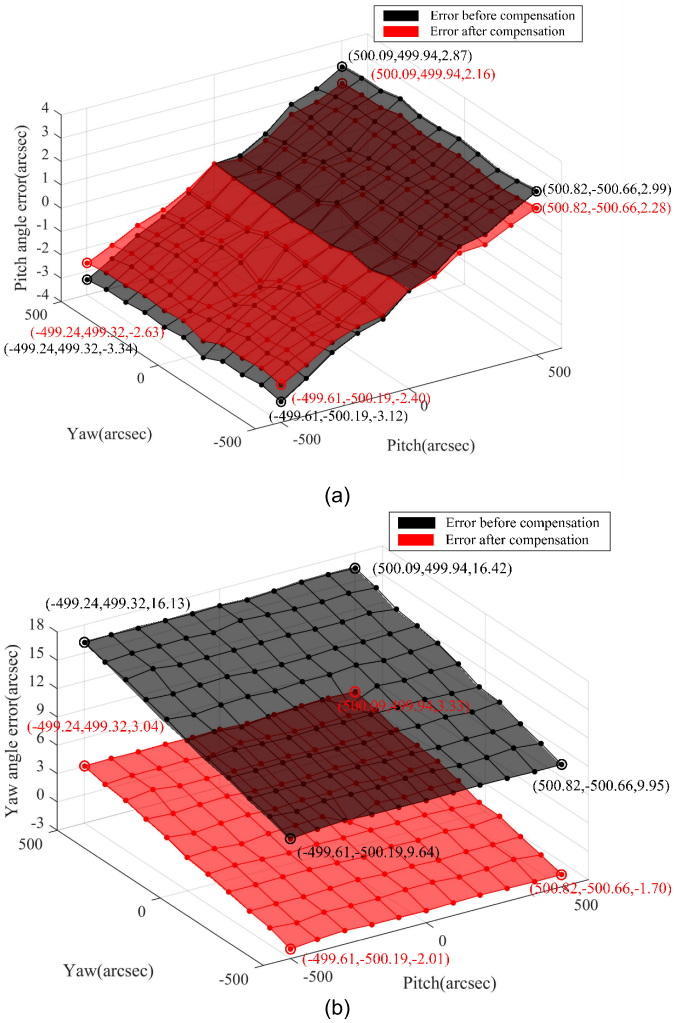

Fig. 12. Results of the accuracy test. (a) Pitch angle error. (b) Yaw angle error.

V. CONCLUSION

To address the systematic error due to autocollimation system aberrations, an influence model of collimating lens aberrations in autocollimation system based on the ray-tracing method was proposed. This model used the ray-tracing method to accurately compute the direction and position of each light ray passing through the collimating lens in the autocollimation system, thereby obtaining the systematic error due to aberrations and eventually improving the accuracy through compensation. Simulations and experiments illustrated that the influence quantity of angular measurement values caused by aberrations reached 0.74 arcsec within the range of ±500 arcsec and that the accuracy could be improved after compensation by using this model. Therefore, researchers can establish their own influence model of any autocollimation system and analyze and compensate for the error caused by aberrations.

In future studies, we will quantitatively analyze various aberrations in collimating lens based on the proposed model and explore the influence of various aberrations with the view of determining the optimization direction of the collimating lens in autocollimation systems.

REFERENCES

[1] Y.-L. Chen et al., "Optical frequency domain angle measurement in a femtosecond laser autocollimator," *Opt. Exp.*, vol. 25, no. 14, pp. 16725–16738, Jul. 2017.
[2] X. R. Tan et al., "Two-dimensional micro-/nanoradian angle generator with high resolution and repeatability based on piezo-driven double-axis flexure hinge and three capacitive sensors," *Sensors*, vol. 17, no. 11, p. 2672, Nov. 2017.
[3] R. P. Li et al., "Cube-corner autocollimator with expanded measurement range," *Opt. Exp.*, vol. 27, no. 5, pp. 6389–6403, Mar. 2019.
[4] J. Y. Wang et al., "Double-grating with multiple diffractions enabled small angle measurement," *Opt. Exp.*, vol. 27, no. 4, pp. 5289–5296, Feb. 2019.
[5] W. Gao, Y. Saito, H. Muto, Y. Arai, and Y. Shimizu, "A three-axis autocollimator for detection of angular error motions of a precision stage," *CIRP Ann.*, vol. 60, no. 1, pp. 515–518, 2011.
[6] S. L. Tan, Y. Shimizu, T. Meguro, S. Ito, and W. Gao, "Design of a laser autocollimator-based optical sensor with a rangefinder for error correction of precision slide guideways," *Int. J. Precis. Eng. Manuf.*, vol. 16, no. 3, pp. 423–431, Mar. 2015.
[7] J. Xue, Z. Qiu, L. Fang, Y. Lu, and W. Hu, "Angular measurement of high precision reducer for industrial robot," *IEEE Trans. Instrum. Meas.*, vol. 70, pp. 1–10, 2021.
[8] F. Siewert et al., "Ultra-precise characterization of LCLS hard X-ray focusing mirrors by high resolution slope measuring deflectometry," *Opt. Exp.*, vol. 20, no. 4, pp. 4525–4536, Feb. 2012.
[9] J. Yellowhair and J. H. Burge, "Analysis of a scanning pentaprism system for measurements of large flat mirrors," *Appl. Opt.*, vol. 46, no. 35, pp. 8466–8474, Dec. 2007.
[10] L. Huang, J. Nicolas, and M. Idir, "Repeatability analysis of one-dimensional angular-measurement-based stitching interferometry," *Opt. Exp.*, vol. 26, no. 16, pp. 20192–20202, Aug. 2018.
[11] P. Huang, Y. Li, H. Y. Wei, L. B. Ren, and S. J. Zhao, "Five-degrees-of-freedom measurement system based on a monolithic prism and phase-sensitive detection technique," *Appl. Opt.*, vol. 52, no. 26, pp. 6607–6615, Sep. 2013.
[12] Y. L. Chen, Y. Shimizu, Y. Kudo, S. Ito, and W. Gao, "Mode-locked laser autocollimator with an expanded measurement range," *Opt. Exp.*, vol. 24, no. 14, pp. 15554–15569, Jul. 2016.
[13] R. P. Li et al., "Roll angle autocollimator measurement method based on a cylindrical cube-corner reflector with a high resolution and large range," *Opt. Exp.*, vol. 30, no. 5, pp. 7147–7161, Feb. 2022.
[14] V. S. Chaudhary, D. Kumar, and S. Kumar, "Gold-immobilized photonic crystal fiber-based SPR biosensor for detection of malaria disease in human body," *IEEE Sensors J.*, vol. 21, no. 16, pp. 17800–17807, Aug. 2021.
[15] G. P. Mishra, D. Kumar, V. S. Chaudhary, and S. Kumar, "Design and sensitivity improvement of microstructured-core photonic crystal fiber based sensor for methane and hydrogen fluoride detection," *IEEE Sensors J.*, vol. 22, no. 2, pp. 1265–1272, Jan. 2022.

[16] V. S. Chaudhary, D. Kumar, G. P. Mishra, S. Sharma, and S. Kumar, "Plasmonic biosensor with gold and titanium dioxide immobilized on photonic crystal fiber for blood composition detection," *IEEE Sensors J.*, vol. 22, no. 9, pp. 8474–8481, May 2022.
[17] V. S. Chaudhary, D. Kumar, and S. Kumar, "SPR-assisted photonic crystal fiber-based dual-wavelength single polarizing filter with improved performance," *IEEE Trans. Plasma Sci.*, vol. 49, no. 12, pp. 3803–3810, Dec. 2021.
[18] G. J. Bergues, C. Schurrer, and N. Brambilla, "Uncertainty determination of the set Nikon 6B autocollimator + visual interface," *IEEE Trans. Instrum. Meas.*, vol. 67, no. 5, pp. 1058–1064, May 2018.
[19] J. Shi, Y. Li, Z. Tao, D. Zhang, H. Xing, and J. Tan, "High-precision autocollimation method based on a multiscale convolution neural network for angle measurement," *Opt. Exp.*, vol. 30, no. 16, p. 29821, 2022.
[20] T. Yandayan, R. D. Geckeler, M. Aksulu, S. A. Akgoz, and B. Ozgur, "Application of advanced shearing techniques to the calibration of autocollimators with small angle generators and investigation of error sources," *Rev. Sci. Instrum.*, vol. 87, no. 5, May 2016, Art. no. 051903.
[21] M. N. Kinnane, L. T. Hudson, A. Henins, and M. H. Mendenhall, "A simple method for high-precision calibration of long-range errors in an angle encoder using an electronic nulling autocollimator," *Metrologia*, vol. 52, no. 2, pp. 244–250, Apr. 2015.
[22] I. A. Konyakhin and A. Smekhov, "Survey of illuminance distribution of vignetted image at autocollimation systems by computer simulation," in *Proc. 8th Int. Symp. Precis. Eng. Meas. Instrum.*, vol. 8759, Jan. 2013, Art. no. 87593F.
[23] I. A. Konyakhin, V. M. Polyakov, and A. M. Vorona, "Research on the methods to compensate the systematic error at optical autoreflection angular measurements," *J. Phys., Conf.*, vol. 48, pp. 932–936, Oct. 2006.
[24] Y. G. Huang, Y. C. Lin, W. Wang, and M. R. Zhao, "Research on the model of photoelectric auto-collimating system based on vector operation," *Laser. Infrared.*, vol. 39, no. 10, pp. 1086–1090, 2006.
[25] F. Zhu, J. B. Tan, and J. W. Cui, "Common-path design criteria for laser datum based measurement of small angle deviations and laser autocollimation method in compliance with the criteria with high accuracy and stability," *Opt. Exp.*, vol. 21, no. 9, pp. 11391–11403, May 2013.
[26] F. Zhu, J. Tan, and J. Cui, "Beam splitting target reflector based compensation for angular drift of laser beam in laser autocollimation of measuring small angle deviations," *Rev. Sci. Instrum.*, vol. 84, no. 6, Jun. 2013, Art. no. 065116.
[27] Y. Shimizu et al., "Ultra-sensitive angle sensor based on laser autocollimation for measurement of stage tilt motions," *Opt. Exp.*, vol. 24, no. 3, pp. 2788–2805, Feb. 2016.

Jian Shi was born in Harbin, China, in 1995. He received the B.S. degree in measurement and control technology and instruments from the Harbin Institute of Technology, Harbin, in 2017, where he is currently pursuing the Ph.D. degree in instrumentation science and technology.

His research interests include angle measurement, autocollimation, and deep learning.

Yuechao Li was born in Dezhou, China, in 1999. He received the B.S. degree in optical information science and engineering from the Harbin Institute of Technology at Weihai, Weihai, China, in 2021. He is currently pursuing the M.S. degree in instrumentation science and technology with the Harbin Institute of Technology, Harbin, China.

His research interests include angle measurement, autocollimation, optical modeling, and simulation.

Daixi Zhang was born in Rizhao, China, in 2001. He is currently pursuing the B.S. degree in precision instruments with the School of Instrumentation Science and Engineering, Harbin Institute of Technology, Harbin, China.

His current research interests include angle measurement, autocollimation, and optical system design.

Heyang Xing was born in Siping, China, in 2001. He is currently pursuing the B.S. degree in measurement and control technology and instruments with the School of Instrumentation Science and Engineering, Harbin Institute of Technology, Harbin, China.

His current research interests include angle measurement, autocollimation, and precision mechanical system design.

Zixi Tao was born in Hunan, China, in June 2001. She is currently pursuing the B.S. degree in precision instruments with the School of Instrumentation Science and Engineering, Harbin Institute of Technology, Harbin, China.

Her current research interests include angle measurement, autocollimation, and digital image processing.

Jiubin Tan received the B.Sc., M.Sc., and Ph.D. degrees in precision instruments and machinery from the Harbin Institute of Technology (HIT), Harbin, China, in 1982, 1987, and 1991, respectively.

Since 1991, he has been with the Department of Instrument Science and Technology, HIT. He was an Elected Member of the Chinese Academy of Engineering, Beijing, China, in 2017. He has 132 granted patents, including 21 international patents. He drafted 26 standards, authored/coauthored more than 310 engineering index and science citation index articles, and authored three monographs. His research interests include precision measurement and instrument technology, ultraprecision optomechatronics equipment technology, and precision laser measurement technology.